IEEE Access
Multidisciplinary | Rapid Review | Open Access Journal

Received February 20, 2019, accepted February 27, 2019, date of publication March 18, 2019, date of current version April 8, 2019.

Digital Object Identifier 10.1109/ACCESS.2019.2905849

Improved Migration Genetic Algorithm Optimization for Variable-Speed Falling Trajectory of Mobile Crossbeam in Composite Hydraulic Press With Pressure Shock

HENG DU[1,2], ZHIQIANG LIN[1,2], YUAN ZHANG[3], HUI CHEN[1,2] AND ZHIMIN XU[4]

[1]School of Mechanical Engineering and Automation, Fuzhou University, Fuzhou 350001, China
[2]Key Laboratory of Fluid Power and Intelligent Electro-Hydraulic Control, Fuzhou University, Fuzhou 350001, China
[3]School of Mechanical and Automotive Engineering, South China University of Technology, Guangzhou 510006, China
[4]Fujian Haiyuan Composites Technology Co., Ltd., Fuzhou 350002, China

Corresponding author: Heng Du (duheng@fzu.edu.cn)

This work was supported in part by the Project of the Fujian College Industry-Academia Cooperation under Grant 2018H6009, and in part by the Project of the Fuzhou Science and Technology Plan under Grant 2016-G-51.

ABSTRACT The optimal design of the mobile crossbeam falling motion control system is an important way to improve the stability of the composite hydraulic press. At present, the falling control strategy is mostly designed by the empirical method, which has the disadvantages of low efficiency and long time. In this paper, a nonlinear hydraulic control system model and three types of falling trajectory mathematical models are established for the mobile crossbeam falling motion control system. Based on the comparison of the motion characteristics of each trajectory, a cubic polynomial falling trajectory which can effectively suppress vibration is designed. This paper proposes a method of trajectory planning based on the spline interpolation function and optimizes the trajectory globally with an improved migration genetic algorithm; the optimized system ITAE index is improved by 49.56% compared with the uniform speed trajectory. The experimental results show that the optimized trajectory's vibration settling time is reduced by 62.91% and the maximum pressure fluctuation is reduced by 25.34% compared with the uniform speed trajectory.

INDEX TERMS Composite hydraulic press, pressure shock, variable-speed falling, trajectory optimization, improved migration genetic algorithm.

I. INTRODUCTION

With the development of advanced materials technology, the molded composites are widely used in the automotive industry [1], aerospace [2], underwater equipment [3], new energy [4] and other high-tech fields because of the advantages such as batch production, high modulus, designable, fatigue resistance and easy to realizing the structure-function integration. Due to its strong point of technology-intensive, high automation and realizing one-time molding and continuous pressing for complex structures, the composite hydraulic presses have become the most important equipment for manufacturing molded materials [5]. However, most composite hydraulic presses are prone to cause vibration during the pressing process, thereby reducing the running smoothness of the mobile crossbeam and aggravating the abrasion of the hydraulic components. It is not conducive to the precision molding of composites, so the effective vibration control for mobile crossbeam is the key to ensure the precision molding of the composite hydraulic press.

At present, there are some solutions for the suppression of hydraulic systems. An *et al.* [6] proposed an extended turned mass damper (ETMD) system combined with control valve to reduce the vibration of the hydraulic system. Pinho *et al.* [7] and Yang *et al.* [8] designed the structure of the relief valve and the pressure retaining valve to improve the vibration suppression performance. Guo *et al.* [9] designed a hydraulic electromagnetic energy-harvesting shock absorber for heavy vehicles to mitigate the vibration of vehicle suspensions. All these researches considered about improving the performance of the hydraulic components However, for composite hydraulic press, these researches can only solve the

The associate editor coordinating the review of this manuscript and approving it for publication was Kuo-Ching Ying.

vibration problem of several types of press, instead of most presses universally. Regarding the composite hydraulic press vibration control, some researches had also made efforts. Cho *et al.* [10] used the open-loop and closed-loop switching controllers to suppress vibration in hydraulic press, and achieved good results. Guo *et al.* [11] proposed a nonlinear cascade controller for the hydraulic press to achieve high-precision, smooth control in the slow pressurization phase. Chen *et al.* [12] developed a predictable multi-modal fuzzy control method for the forging hydraulic press to make the slider position smoothly at high speed. Those researches suppress vibration well, but for large-tonnage composite hydraulic presses, the current anti-vibration technology has large scale of experiment and high cost. Meanwhile, composite hydraulic press, a large inertia system, is easy to generate vibration caused by the addition of closed-loop feedback when the mobile crossbeam falls, and even further aggravates the press vibration. So it's not suitable for engineering application.

Because of high pertinence and the ability of obtaining the optimal solution in advance, trajectory planning technology can avoid large-scale experiments and easily implement in engineering It has been applied in industrial manipulator [13], elevator [14], underwater equipment [15] aircraft [16] and other fields to suppress vibration Many researches had used trajectory planning to solve structural vibration problems Moriello *et al.* [17] reduces vibration of industrial manipulator using exponential B-spline trajectories generated by dynamic filters. Aribowo and Terashima [18] proposed the free via points using cubic spline optimization with combined with input shaping to reduce motion time and vibration of robot arms. Subbarao and Shippey [19] proposed a hybrid genetic algorithm collocation method directly optimizing the trajectory to solve the constraint optimal control problem of spacecraft. Li *et al.* [20] used an improved genetic algorithm to optimize the B-spline curve parameters, enabling intelligent vehicles to operate stably in high-speed driving conditions. All those researches solve the structural vibration problem well by optimizing the motion trajectory of mechanical structures, and they are easier to implement in engineering. However, most composite hydraulic presses use the proportional valve open-loop control mode when the mobile crossbeam falls, the nonlinearity of the hydraulic system must be taken into consideration. Ren *et al.* [21] used a trajectory planning method based on the fifth degree B-spline interpolation trajectory to realize the smooth movement of 3DOF electro-hydraulic servo manipulators. For the hybrid mechanical press, He *et al.* [22], used the trajectory planning method based on inverse kinematics and cubic spline interpolation to track punch trajectory well. Both researches comprehensively consider the characteristics of hydraulic and mechanical systems, and the trajectory tracking effect is good. They have a good reference value for the vibration suppression of the composite press mobile crossbeam in this paper However, they are both small inertia hydraulic systems only considering the trajectory planning of the actuator, and they don't need to consider the pressure vibration suppression inside the actuator because of the small inertia. However, the inertia of composite hydraulic press mobile crossbeam is very large, and the press performance can be easily affected by a large pressure shock generating during the falling process, thereby affecting the product quality. Therefore, it is necessary to comprehensively consider the mechanical and hydraulic vibration suppression in order to reduce the rigid impact, flexible impact and pressure shock in the optimization. It puts forward new requirements for the trajectory planning of the composite press mobile crossbeam.

The rest of the paper is structured as follows: The main content of section 2 is establishing a composite hydraulic press mobile crossbeam nonlinear hydraulic model and using neural network for model identification. Section 3 concludes three types of mobile crossbeam falling trajectory models, trajectory motion characteristics simulation and optimization for the cubic polynomial trajectory using improved migration genetic algorithm. The main content of section 4 is establishing a mobile crossbeam variable-speed falling system experiment platform to verify the reliability of the established model and the effectiveness of the optimized trajectory. Conclusions are drawn in Section 5.

II. PROBLEM DESCRIPTION AND MODEL BUILDING

A. WORKING PRINCIPLE OF COMPOSITE HYDRAULIC PRESS

As shown in Fig. 1, the composite hydraulic press mainframe is the large-scale three-beam four-column structure, the body is fixed on the lower beam, and the upper beam is fixed on the lower beam through four support rods. A tie rod is arranged inside the support beam to generate the overall pre-tightening force of the frame. Pumping station is arranged above the press, and the double-return cylinder is controlled in real time to prevent motion shock when the mobile crossbeam falls. During the product pressing process, double master cylinders provide main pressing force, and the leveling device levels the slider. A working cycle of composite press mainly includes quick falling, fast turn slow, slow falling, leveling

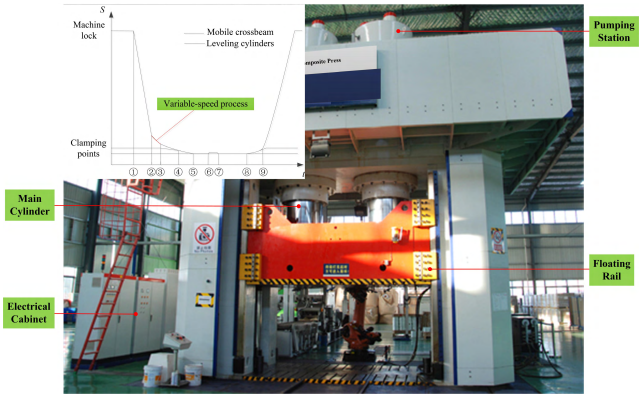

FIGURE 1. Schematic diagram of composite hydraulic press and displacement curve of mobile crossbeam.

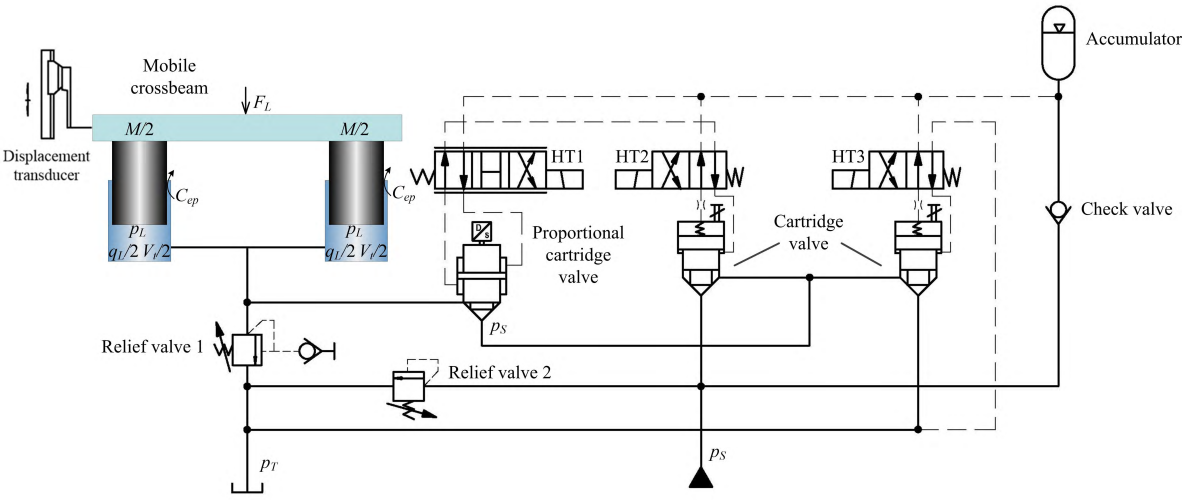

FIGURE 2. Schematic diagram of the mobile crossbeam falling hydraulic control system.

(with pressure), molding and clamping pressure, maintaining pressure, micro mold opening, second pressing, pressure relief, unloading and return stroke. ⑤-⑧ is the molding, maintaining pressure and mold opening stage of the press. It is the main working stage of compression molding, and it takes most of the time for the press during working, ②-③ is the mobile crossbeam falling fast turn slow stage, it's the key to achieve the impactless speed switching and improve the product quality. In this stage, the mobile crossbeam needs to achieve a quick transition of the falling speed from fast to slow in a short time, and the press cannot have obvious hydraulic shock and vibration.

Fig. 2 is the schematic diagram of the crossbeam falling hydraulic system [23]. During falling, the electromagnet HT3 is energized, the controller sends a target signal to the proportional electromagnet HT1 to control the proportional cartridge valve opening. It changes the falling speed to realize the falling motion control of the mobile crossbeam. The falling motion is the basic premise and important foundation for the flexible docking of sliding block and leveling cylinder. It is also the key link of vibration suppression, and its motion performance directly affects the pressing performance of the hydraulic press. Therefore, it is necessary to design a trajectory to minimize the vibration generated by the press during working process.

B. ESTABLISHING MOBILE CROSSBEAM VARIABLE-SPEED FALLING SYSTEM MODEL

During the mobile crossbeam variable-speed stage, the press variable-speed system mainly controls two symmetrical return cylinders by a three-way proportional cartridge valve, thereby realizing the transition of fast falling speed to slow. In order to deeply analyze the motion characteristics, two return cylinders can be equivalent to a plunger cylinder. Then we establish the mobile crossbeam variable-speed falling mathematical model based on kinematics and dynamics analysis.

1) DYNAMIC EQUATION OF VARIABLE-SPEED FALLING SYSTEM

As shown in Fig. 2, It is assumed that the two return cylinders are completely symmetrical and have the same parameters, the influence of pipeline loss and temperature on oil viscosity are ignored. The dynamic equation of valve control plunger cylinder is listed as follows:

$$q_L = C_d x_v w \sqrt{\frac{2(p_L - p_T)}{\rho}} \tag{1}$$

$$q_L = A_p \frac{dx_p}{dt} - C_{ep} p_L - \frac{V_t}{\beta_e} \frac{dp_L}{dt} \tag{2}$$

$$A_p p_L = F_L - M \frac{d^2 x_p}{dt^2} - B_p \frac{dx_p}{dt} - K x_p \tag{3}$$

where q_L is the load flow, A_p is the area of non-rod end chamber p_L is the pressure of non-rod end chamber p_T is the return pressure, β_e is the effective volumetric modulus of elasticity, C_{ep} is the external leakage coefficient of hydraulic cylinder, F_L is the gravity of the mobile crossbeam, M is the total mass of piston and load converted to piston K is the load spring stiffness, x_p is the displacement of return cylinder B_p is the viscous damping coefficient of loads and pistons.

Equation. (1) is the flow equation with valve core displacement as input, and we set the target valve core displacement as x_v:

$$\begin{cases} q_N = C_d x_N w \sqrt{\frac{2\Delta p_N}{\rho}} \\ q_L = C_d x_v w \sqrt{\frac{2\Delta p}{\rho}} \end{cases} \tag{4}$$

where q_N is the cartridge valve nominal flow, C_d is the flow coefficient; p is the hydraulic oil density, Δp_N is the cartridge valve nominal pressure drop Δp is the differential pressure

between proportional valve A-T port, $\Delta p = p_L - p_T$, x_N is the valve opening corresponding to nominal flow, x_v is the valve core displacement, w is the cartridge valve area gradient.

According to (4), we can derive:

$$q_L = q_N \sigma \sqrt{\frac{\Delta p}{\Delta p_N}} \tag{5}$$

where σ is the ratio of target valve port opening and rated opening, $\sigma = x_v / x_N$.

According to the proportional cartridge valve sample, the given spool voltage is approximately proportional to the valve opening in the working area so it is considered as a proportional link.

$$\begin{cases} u_t = K_u x_v \\ u_N = K_u x_N \end{cases} \tag{6}$$

where u_t is the system input voltage; u_N is the system rated voltage; K_u is the electromagnetic amplification coefficient of proportional valve.

Bringing (6) into (5) to get:

$$q_L = q_N \frac{u_t}{u_N} \sqrt{\frac{\Delta p}{\Delta p_N}} \tag{7}$$

2) STATE SPACE EQUATION OF VARIABLE-SPEED FALLING SYSTEM

In order to facilitate subsequent design analysis, the above model is transformed into state space equation. Select x_p, the rod speed $\dot{x}_p$ and p_L as state variables, i.e. $x = [x_p, \dot{x}_p, p_L]^T$. Select u_t and F_L as system inputs, i.e. $U = [u_t,\ F_L]^T$. Select p_L, x_p and $\dot{x}_p$ as system output, i.e. $y = [x_p, \dot{x}_p, p_L]^T$. The nonlinear dynamic equations of variable-speed falling system can be obtained by combining (2), (3) and (7):

$$\begin{cases} \dot{x} = Ax + g(x)U \\ y = Ix \end{cases} \tag{8}$$

$$\text{where } A = \begin{bmatrix} 0 & 1 & 0 \\ -\frac{K}{M} & -\frac{B_p}{M} & -\frac{A_p}{M} \\ 0 & \frac{\beta_e A_p}{V_t} & \frac{\beta_e C_{ep}}{V_t} \end{bmatrix}; I = \begin{bmatrix} 1 & 0 & 0 \\ 0 & 1 & 0 \\ 0 & 0 & 1 \end{bmatrix};$$

$$g(x) = [g_1(x) \quad g_2(x)];$$

$$g_1(x) = \begin{bmatrix} 0 & 0 & -\frac{\beta_e q_N}{V_t u_N} \sqrt{\frac{p_L - p_T}{\Delta p_N}} \end{bmatrix}^T;$$

$$g_2(x) = \begin{bmatrix} 0 & \frac{1}{M} & 0 \end{bmatrix}^T;$$

$$V_t = V_1 - A_p x_p.$$

In the above equations, V_t is the effective volume of non-rod end chamber, which changes in real time with x_1. V_1 is the volume of non-rod end chamber

TABLE 1. Model identification experiment data.

Voltage (V)	Crossbeam falling speed (m/s)	Pressure (MPa)
1	0.016	7.5
1.5	0.025	7.5
2	0.034	7.5
2.5	0.053	7.46
3	0.084	7.4
3.5	0.124	7.33
4	0.170	7.2
4.5	0.217	7.13
5	0.264	6.97
5.5	0.312	6.87
6	0.355	6.695
6.5	0.392	6.59
7	0.429	6.45
7.5	0.458	6.29
8	0.482	6.11
8.5	0.505	6.11
9	0.519	5.95
9.5	0.534	5.94
10	0.546	5.88

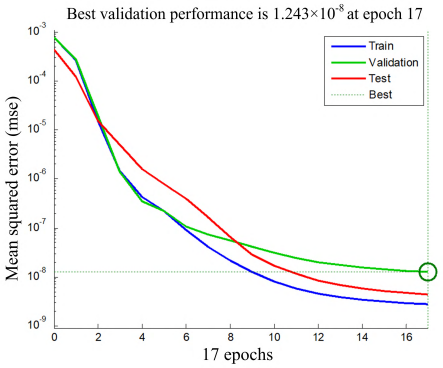

FIGURE 3. Neural network training results mean variance.

C. MODEL IDENTIFICATION BASED ON NEURAL NETWORK

The state space model established above can characterize the dynamic characteristics of the system to a certain extent. However, the hydraulic press system has a series of uncertain factors such as: hysteresis dead zone caused by valve wear and loss of oil pipe along the path. Aiming at the problems of partial model uncertainty, high nonlinearity and complicated working conditions of the actual falling beam system of the press, this paper uses BP neural network algorithm [24] to train the measured data, and improve the ability of model to characterize the dynamic characteristics of hydraulic press. The measured data are as follows:

Taking the voltage u_t as input, the system load flow q_L as output, the model is trained by the neural network algorithm. The number of hidden layer neurons is set to 3, the training sample accounts for 70% of the total samples, and the testing samples and verification samples each account for 15% of the total number of samples. So the following figure can be obtained:

It can be seen from Fig. 3 that after 17 epochs of training, the variance of the neural network training verification results

can reach 1.243×10^{-8}, which can realize the higher precision mapping of the training model to the actual system.

III. SIMULATIONS AND IMPROVED MIGRATION GENETIC ALGORITHM OPTIMIZATION

A. MATHEMATICAL DESCRIPTION AND SIMULATIONS

When the mobile crossbeam falls, it is necessary to switch from one speed to another within a certain time. Therefore, there are many possibilities for the falling trajectory.

1) ESTABLISHING VARIABLE-SPEED FALLING TRAJECTORY MODEL

At present, trajectory used widely include the uniform speed trajectory, the cubic and high-order polynomial trajectory, the B-spline trajectory, and the simple harmonic trajectory [25]–[27] Among them, the high-order polynomial trajectory and the simple harmonic trajectory are excellent choices for the mobile crossbeam due to the advantages of high-order derivative continuous, simple structural form and good smoothness. They could avoid the flexible impact and rigid impact well during falling.

a: OPTIMIZED PARAMETER DESIGN

The hydraulic press uses the Atos LIQZO-LE-503L4/Q three-way proportional valve as the control component of the mobile crossbeam variable-speed falling system. In ideal conditions, when the pressure drop at valve port is constant, the input voltage signal and the oil flow rate of valve have the following relationship:

$$q_L = \begin{cases} \lambda_{q1}u, & -2 \le u \le 2 \\ \lambda_{q2}u - q_0\ \mathrm{sgn}(u), & 2 \le |u| \le 10 \end{cases} \tag{9}$$

where λ_{qi} is the voltage-flow coefficient of valve, q_0 is the additional flow.

As shown in Fig. 4:

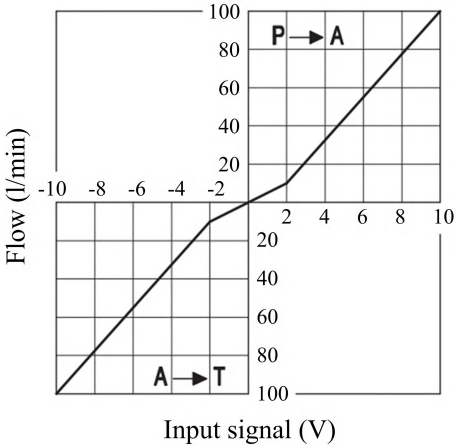

FIGURE 4. Three-way proportional valve flow curve.

The flow through valve and actuator speed has the following relationship:

$$q_L = A_n v \tag{10}$$

where A_n is the effective working area of actuator.

Based on the open-loop control mode during the mobile crossbeam falling process, the input signals of valve shown in (9) and (10) have good linear relationship with actuator motion speed. The method of optimizing valve input command signal can be used to optimize the velocity and trajectory of the mobile crossbeam during falling process.

b: ESTABLISHING TRAJECTORY MODEL

In order to enable the mobile crossbeam to switch speed rapidly and smoothly, the initial and terminal boundary conditions of the trajectory are defined as follows:

$$U(t_0) = u_0 \quad U(t_s) = u_t \tag{11}$$

$$\dot{U}(t_0) = \alpha_0 \quad \dot{U}(t_s) = \alpha_t \tag{12}$$

where u_0 is the voltage command of the mobile crossbeam at the starting point of variable-speed falling process, u_t is the voltage command of the mobile crossbeam at the ending point of variable-speed falling process, α_0 and α_t are the first derivative of voltage command at initial and terminal points of the variable-speed falling process. Then, establish the mobile crossbeam variable-speed falling trajectory.

Uniform speed trajectory:

$$U_{uni}(t) = u_0 + \frac{u_t - u_0}{t_s}t \tag{13}$$

Simple harmonic trajectory:

$$U_{shm}(t) = \frac{u_0 - u_t}{2}\cos\left(\frac{\pi}{t_s}t + 2k\pi\right) + \frac{u_0 + u_t}{2} \tag{14}$$

where k is the number of harmonic oscillation cycles in the variable-speed process, $k = 0_{\circ}$.

Cubic polynomial trajectory:

$$U_{poly}(t) = u_0 + (u_t - u_0)\left(3\left(\frac{t}{t_s}\right)^2 - 2\left(\frac{t}{t_s}\right)^3\right) \tag{15}$$

2) SIMULATIONS AND ANALYSIS

According to the craft requirements of the mobile crossbeam variable-speed falling process, the target voltage command is set to decrease from 10V to 3V in variable-speed period, and the command voltage change rate at the initial and terminal points is zero. So:

$$U(t_0) = 10\mathrm{V} \quad U(t_c) = 3\mathrm{V} \tag{16}$$

$$\dot{U}(t_0) = 0 \qquad \dot{U}(t_c) = 0 \tag{17}$$

where, $t_c = t_s + t_0$. Inputting (16) and (17) into (13) to (15), the target trajectory with boundary conditions can be obtained.

Set simulation time as $0 \sim 4$s, and when $t = 0 \sim 1$s, the input voltage command is 10V. The variable-speed initial point time is $t_0 = 1$s and when $t = t_0 \sim t_c$ the input voltage is a signal command along specified trajectory within the boundary condition range. When $t = t_c \sim 4$s, the input voltage command is 3V.

Other simulation parameters are shown in the table below:

TABLE 2. Simulation parameter.

Parameter name	Symbol	Value	Unit
Total mass of piston and load converted to piston	M	40000	kg
Return cylinder stroke	L	2.275	m
Gravity of the press	F_L	3.92×10^5	N
Effective volumetric modulus of elasticity	β_e	7×10^8	Pa
External leakage coefficient of hydraulic cylinder	C_{ep}	7.1×10^{-17}	$m^5/(N\cdot s)$
Viscous damping coefficient	B_p	167406.57	N·s/m
Area of non-rod end chamber	A_p	0.05089	m^2
Load spring stiffness	K	0	N/m
Cartridge valve nominal flow	q_N	1100	L/min
Cartridge valve nominal pressure drop	Δp_N	10	bar
Return pressure	p_T	0	bar
System rated voltage	u_N	10	V
Volume of non-rod end chamber	V_1	3.5×10^{-3}	m^3

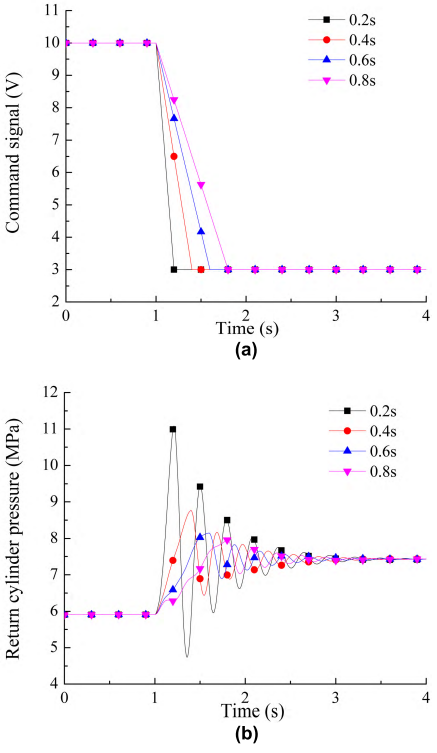

FIGURE 5. Uniform speed trajectory pressure fluctuation. (a) Command trajectory. (b) Return cylinder pressure fluctuation.

a: INFLUENCE OF VARIABLE-SPEED TIME ON PRESSURE CHARACTERISTICS

According to the craft requirements of the mobile crossbeam fast turn slow process, the variable-speed time is generally within 1s, so we set the variable-speed times at 0.2s,0.4s,0.6s and 0.8s

Fig. 5 to Fig. 7 are the system pressure curves about three trajectory voltage signals decrease from 10V to 3V. It can be seen that the overall change rate of three trajectories

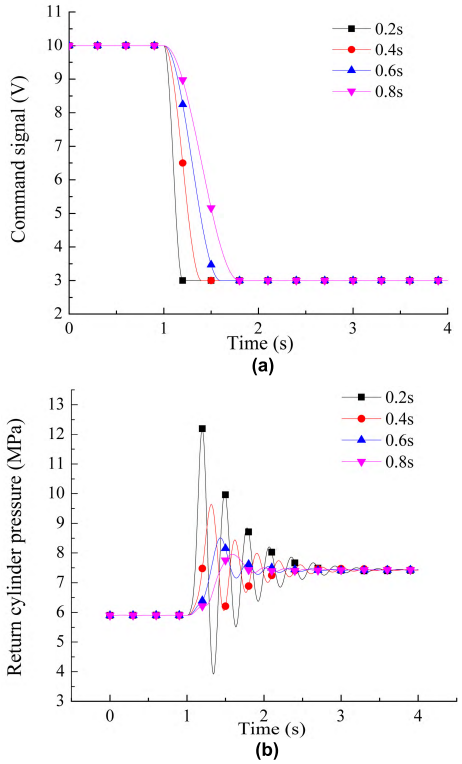

FIGURE 6. Simple harmonic trajectory pressure fluctuation. (a) Command trajectory. (b) Return cylinder pressure fluctuation.

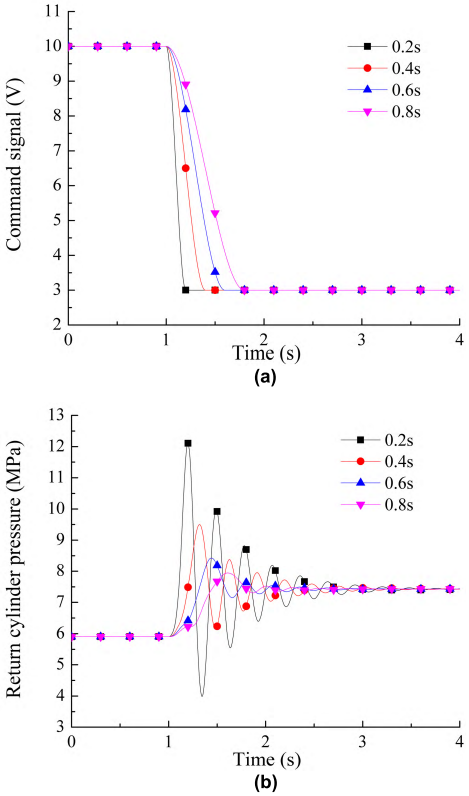

FIGURE 7. Cubic polynomial trajectory pressure fluctuations. (a) Command trajectory. (b) Return cylinder pressure fluctuation.

gradually becomes slower, and the return cylinder pressure fluctuations gradually decrease as the variable-speed time increases.

It can be seen from Fig. 8 that during the variable-speed process, the return cylinder pressure fluctuation of each trajectory gradually decreases as the variable-speed time increases. When variable-speed time is 0.2s, the system maximum overshoot of the simple harmonic trajectory and the cubic polynomial trajectory is higher than the uniform speed trajectory. When the variable-speed time is 0.8s, the system pressure maximum overshoot of three trajectories gradually reach consensus.

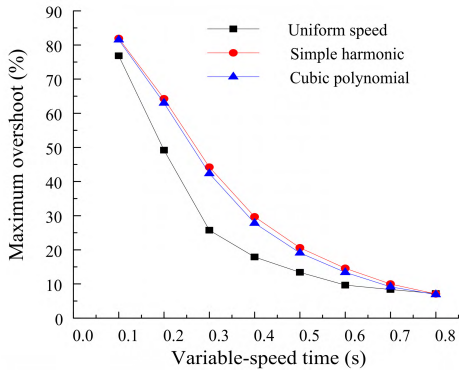

FIGURE 8. Pressure fluctuation overshoots.

It can be seen from Fig. 9 that the settling time is substantially the same when the variable-speed time is 0.2s. The settling time of uniform speed trajectory in 0.2s $\sim$ 0.45s is smaller than the other trajectories. When the variable-speed time exceeds 0.45s, the settling time of the simple harmonic trajectory and the cubic spline trajectory is rapidly reduced. Overall, the settling time of system is shortened as the variable-speed time increases.

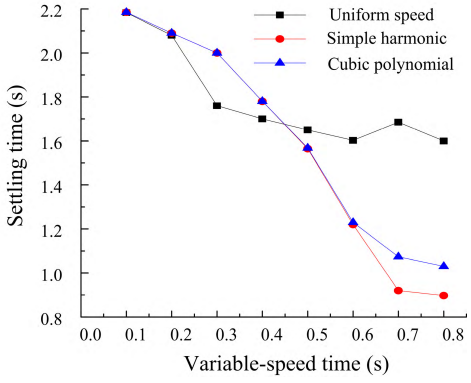

FIGURE 9. Pressure fluctuation settling time.

As can be seen from Fig. 10, when the variable-speed time is 0.2 s, the number of oscillation is substantially the same. As the variable-speed time increases, system settling times of three trajectories gradually decreases, and the number of oscillation of the simple harmonic trajectory and the cubic polynomial trajectory is less than the uniform speed trajectory.

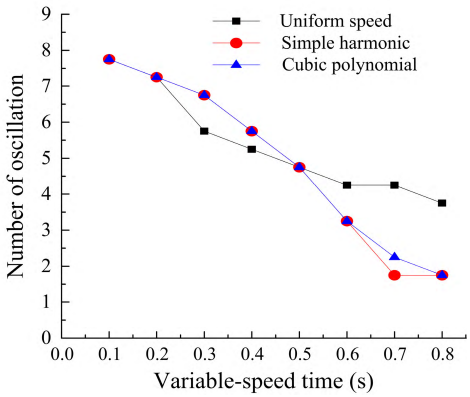

FIGURE 10. Pressure fluctuation oscillations.

The integrated time and absolute error (ITAE) is a relatively balanced system response performance index [28], which combines the comprehensive characteristics of settling time and deviation. The system designed with this index has small system deviation and short settling time. The following formula is the ITAE indicator expression:

$$J = \int_0^{t_s} t|e(t)dt \tag{18}$$

where $e(t)$ is the deviation of transition pressure and new steady state pressure, t_s is the settling time of variable-speed falling process.

It can be seen from Fig. 11 that the ITAE index falls fastest in the early stage, which indicates that the system pressure fluctuation decreases rapidly as the variable-speed time increases. The system ITAE index is lowest between 0.6 and 0.7s. However, after 0.7s, the system ITAE index of each trajectory gradually rises as the variable-speed time increases. It indicates that when the system variable-speed time exceeds a certain limit, the integral of the pressure deviation and time multiplication increases, and the system overall tracking performance decreases. But the tracking performance of the simple harmonic trajectory and the cubic polynomial trajectory is better than the uniform speed trajectory.

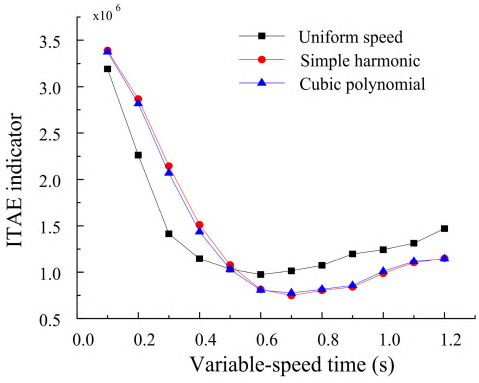

FIGURE 11. Pressure fluctuation ITAE index.

b: INFLUENCE OF DIFFERENT TRAJECTORIES ON PRESSURE CHARACTERISTICS

According to the analysis of the system ITAE index, the system pressure response of three trajectories has a relatively balanced performance when $t_s = 0.6$s. Simulation analysis of the system pressure fluctuation response performance of three trajectories is as follows:

It can be seen from Fig. 12 that the maximum overshoot of the uniform speed trajectory pressure response is small, but the number of oscillation and the settling time are long, and the amplitude damps slowly when $t_s = 0.6$s. Combining (9) and (10), the first derivative of command voltage reflects the acceleration when the mobile crossbeam falls, and the second derivative reflects the jerk. During falling, the simple harmonic trajectory and the cubic polynomial trajectory have better high-order smoothness over the entire stroke. But the command signal curve has vertices when the uniform speed trajectory is at $t_s = 1.0$s and $t_s = 1.6$s, the second derivative of voltage signal tends to infinity. This reflects that the uniform speed trajectory is prone to generate acceleration sudden changes at endpoints, which leads to the system flexible impact.

Therefore, the simple harmonic trajectory and the cubic polynomial motion trajectory are better than the uniform speed trajectory. Besides, the boundary conditions of the cubic polynomial trajectory can be parameterized freely, which is more convenient for engineering application.

B. ESTABLISHING VARIABLE-SPEED FALLING TRAJECTORY BASED ON CUBIC SPLINE INTERPOLATION

The cubic spline interpolation trajectory is an interpolation function based on the Hermite interpolation polynomial, which is essentially a piecewise curve. The functions on each segment are cubic polynomial and have second derivative continuity at the connecting points, so the cubic spline interpolation trajectory has good stability and convergence [29]. In the mobile crossbeam variable-speed falling system, the trajectory can be divided into finite equidistant segments, let $t = t_0, t_1, \ldots, t_n$, thereby dividing into some small segments the trajectory:

$$U_{spl}(t) = \begin{cases} \sum_{i=0}^{m} \varphi_{0,i} t^i, & t \in [t_0, t_1] \\ \vdots & \vdots \\ \sum_{i=0}^{m} \varphi_{j,i} t^i, & t \in [t_j, t_{j+1}] \\ \vdots & \vdots \\ \sum_{i=0}^{m} \varphi_{n-1,i} t^i, & t \in [t_{n-1}, t_n] \end{cases} \tag{19}$$

where $j = 0, 1, \ldots, n-1, m = 3$. It can be seen from (19) that $U_{spl}(t)$ has 4 undetermined coefficients on each minizone $[t_j, t_j + 1]$, which are divided into n segments, so a total of 4 n parameters need to be determined. Given the function value of the cubic spline interpolation function on each node:

$$U_{spl}(t_j) = u_j, \quad j = 0, 1, \ldots, n \tag{20}$$

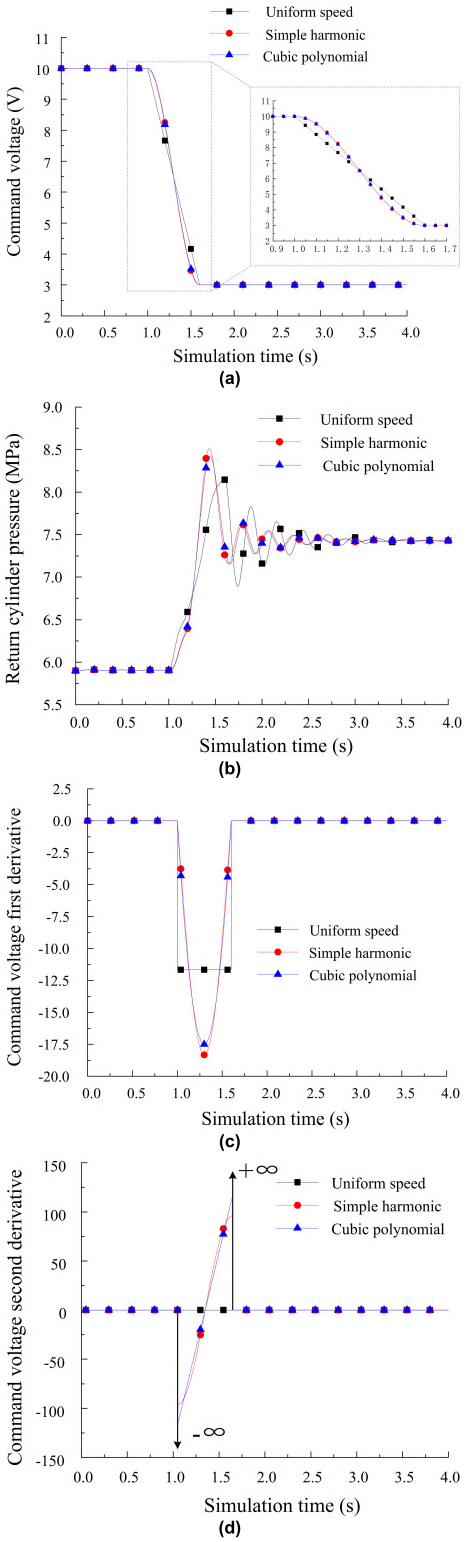

FIGURE 12. Variable-speed motion characteristics of each trajectory. (a) Input valve target command. (b) Return cylinder pressure fluctuation. (c) Command voltage first derivative. (d) Command voltage second derivative.

According to the definition of cubic spline interpolation function, the function values are equal at each node of the piecewise function, and the same as first and second derivatives.

$$\begin{cases} U_{spl}\left(t_j^-\right) = U_{spl}\left(t_j^+\right) \\ \dot{U}_{spl}\left(t_j^-\right) = \dot{U}_{spl}\left(t_j^+\right) \\ \ddot{U}_{spl}\left(t_j^-\right) = \ddot{U}_{spl}\left(t_j^+\right) \end{cases}, \quad j = 1, 2, \ldots, n-1 \tag{21}$$

From (20), $n+1$ equations can be obtained, (21) can obtain 3 $n-3$ equations. So there are 4 $n-2$ conditional equations totally, two more equations are needed to determine $U_{spl}(t)$. According to the process requirements of variable-speed falling motion, we use the first type of boundary condition of interpolation function, that is, the first-order derivative value of the two endpoints of interpolation function is already known:

$$\dot{U}_{spl}(t_0) = \alpha_0, \quad \dot{U}_{spl}(t_n) = \alpha_n \tag{22}$$

Based on [30] and [31], the cubic spline interpolation $U_{spl}(t)$ can be solved.

C. IMPROVED GENETIC ALGORITHM TRAJECTORY OPTIMIZATION BASED ON MIGRATION THEORY

Genetic Algorithms (GA) is proposed Professor Holland of Michigan University. It's a global parallel stochastic optimization algorithm simulating the natural biological evolution theory [32], [33].

However, the Standard Genetic Algorithm (SGA) has single population diversity, and it is easy to converge to the local optimal solution rather than the global, which results in the "premature" phenomenon. It greatly restricts the optimization efficiency and global optimization ability of the algorithm. In recent years, scholars have used the natural phenomenon of migration theory and colonial competition to improve the SGA, and proposed the parallel GA mode based on migration theory [34]–[36]. According to the actual mathematical model, this paper uses the multi-island migration GA to optimize the floating value of each cubic spline interpolation trajectory segment node and look for a set of design variables that optimize performance indicators.

1) VARIABLE-SPEED FALLING TRAJECTORY OPTIMIZATION

Based on the spline interpolation trajectory, we use the migration genetic algorithm combined with multi-strategy to optimize the variable-speed falling trajectory, and take the minimum ITAE index of the return cylinder pressure fluctuation as the goal. In consideration of each constraint, let computer search for the floating value Δu_j of finite connecting points in the feasible space globally.

Build the optimization model:

$$\min f(\tilde{p}) \tag{23}$$

$$s.t. \begin{cases} U_{\min} \le u(t) \le U_{\max} \\ \dot{U}_{\min} \le \dot{u}(t) \le \dot{U}_{\max} \\ \Delta U_{\min} \le \Delta u_j \le \Delta U_{\max} \end{cases} \tag{24}$$

where $U_{\min}$, $U_{\max}$ denote as the maximum and minimum values of variable-speed falling command. $\dot{U}_{\min}$, $\dot{U}_{\max}$ express as the Maximum and minimum values of the change rate of variable-speed falling command. $\Delta U_{\min}$, $\Delta U_{\max}$ are the maximum and minimum values of node float. f(·) is the objective function to be optimized. In this paper, f(·) stands for $U_{spl}(t)$.

Build the system fitness function:

$$J(\tilde{p}, u) = \int_0^{t_s} t|e(t)|dt + \sum_{i=1}^{m} r_i P_i(u) \tag{25}$$

where r_i is the penalty factor for each penalty term. $P_i(u)$ is the penalty items corresponding to each constraint.

There are many forms of penalty function, it usually adds to the original objective function by the addition form as shown in (25). Then construct the specific punishment functions:

$$P_1(u) = \begin{cases} |U_{\min} - \min u(t)|, & \min u(t) \le U_{\min} \\ 0, & \text{others} \end{cases} \tag{26}$$

$$P_2(u) = \begin{cases} |U_{\max} - \max u(t)|, & \max u(t) \ge U_{\max} \\ 0, & \text{others} \end{cases} \tag{27}$$

$$P_3(u) = \begin{cases} \left|\dot{U}_{\min} - \min \dot{u}(t)\right|, & \min \dot{u}(t) \le \dot{U}_{\min} \\ 0, & \text{others} \end{cases} \tag{28}$$

$$P_4(u) = \begin{cases} \left|\dot{U}_{\max} - \max \dot{u}(t)\right|, & \max \dot{u}(t) \ge \dot{U}_{\max} \\ 0, & \text{others} \end{cases} \tag{29}$$

$$P_5(u) = \begin{cases} \left|\Delta U_{\min} - \min \Delta u_j(t)\right|, & \min \Delta u_j(t) \le \Delta U_{\min} \\ 0, & \text{others} \end{cases} \tag{30}$$

$$P_6(u) = \begin{cases} \left|\Delta U_{\max} - \max \Delta u_j(t)\right|, & \max \Delta u_j(t) \ge \Delta U_{\max} \\ 0, & \text{others} \end{cases} \tag{31}$$

where $t \in [t_0, t_c]$, $\max u(t)$ and $\min u(t)$ are the maximum and minimum values of the mobile crossbeam falling command signal, $\max \dot{u}(t)$ and $\min \dot{u}(t)$ denote as the maximum and minimum values of the change rate of the mobile crossbeam falling command signal, $\max \Delta u_j(t)$ and $\min \Delta u_j(t)$ denote as the maximum and minimum values of node float.

The flow chart of the migration genetic algorithm is as follows:

2) TRAJECTORY OPTIMIZATION RESULTS

Based on the actual system requirements, the parameters of the variable-speed falling optimization process are shown in Table. 3:

If the segments of the cubic spline interpolation trajectory and the search space are too small, it is difficult to find the global optimal trajectory. But the excessive segments will greatly increase the calculation difficulty and reduce the search efficiency. Because the variable-speed time is usually within 1s, it is short, we optimize the trajectory divided into 2 $\sim$ 5 segments separately, and optimize each segment

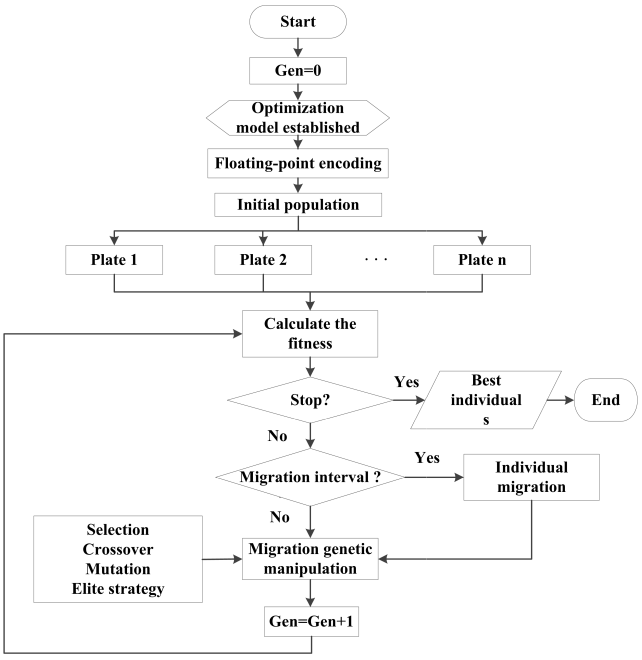

FIGURE 13. Flow chart of migration genetic algorithm.

TABLE 3. Optimization parameter.

Parameter name	Symbol	Value	Unit
Initial voltage	$U_{spl}(t_0)$	10	V
Terminal voltage	$U_{spl}(t_c)$	3	V
Initial command change rate	$\dot{U}_{spl}(t_0)$	0	V/s
Terminal command change rate	$\dot{U}_{spl}(t_c)$	0	V/s
Variable-speed time	t_s	0.6	s
Maximum command change rate	$\dot{U}_{\max}$	0	1
Minimum command change rate	$\dot{U}_{\min}$	0	1
Maximum voltage	$U_{\max}$	10	V
Minimum voltage	U_{min}	3	V
Maximum command floating value	$\Delta U_{\max}$	7	V
Minimum command floating value	$\Delta U_{\min}$	-7	V
Penalty factor	r_i	1.0×10 6	1
Sampling period	τ	0.001	s

multiple times. Finally, it can be concluded that better results can be obtained when using 3-segment form according to Table 3.

The optimization process is shown in Fig. 14. It can be seen that, the group individuals are dispersed, the average fitness of the population is larger, and the fitness value of best individuals in the first generation is about 1.8×10^6 during the early evolution process. During the 1st to 8th generations of reproduction, each island population promotes

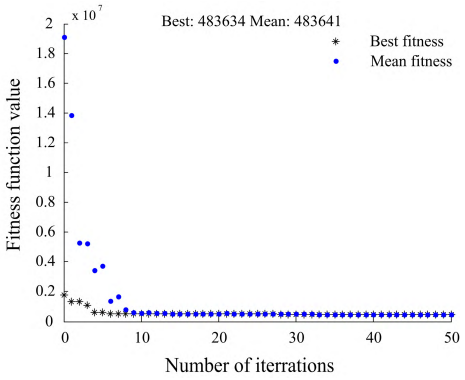

FIGURE 14. Migration genetic algorithm optimization iterative process.

the population to produce more excellent individuals through individual competition, gene mutation and migration operations, and gradually converges to optimal solutions. From the 8th generation to the 50th generation, the individuals on each island are very close to the optimal solution, and evolve to the 50th generation with the constraint of minimum tolerance. Then the algorithm ends.

The optimized floating value of trajectory node is:

$$\Delta u_1 = -0.32 \quad \Delta u_2 = -1.214 \tag{32}$$

The optimized trajectory is:

$$U_{spl}(t) = \begin{cases} 183.9412t^3 - 103.1179t^2 + 10, & 0 \le t \le 0.2 \\ 39.7374(t-0.2)^3 + 7.2468(t-0.2)^2 & \\ \quad -19.1742(t-0.2) + 7.3468, & 0.2 \le t \le 0.4 \\ -7.7392(t-0.4)^3 + 31.0893(t-0.4)^2 & \\ \quad -11.507(t-0.4) + 4.1197, & 0.4 \le t \le 0.6 \end{cases} \tag{33}$$

Inputting the optimized trajectory into the model (8), we can get the following figures:

It can be seen from Fig. 15(a) that displacement curve before optimization will produce a fluctuation between 1s and 2s, and the optimized curve is smoother. After 1.6s, two curves tend to be parallel, and the falling speed of mobile crossbeam has reached the setting speed. From Fig. 15(b) that during the variable-speed process of 1s-1.6s, the displacement stroke of the mobile crossbeam before optimization is 0.22m, and the optimized is 0.19m. It shows that the optimized variable-speed trajectory can switch the mobile crossbeam speed in a short stroke rapidly. This can shorten the stroke of the entire pressing process and relatively reserve more strokes for the leveling process.

As can be seen from Fig. 16, both the uniform speed trajectory and the optimized trajectory can reduce the mobile crossbeam falling speed from 0.545 m/s to 0.083 m/s. However, taking the uniform speed trajectory as the falling trajectory make the speed large fluctuations near the new steady state, and the settling time is long and difficult to be stable rapidly.

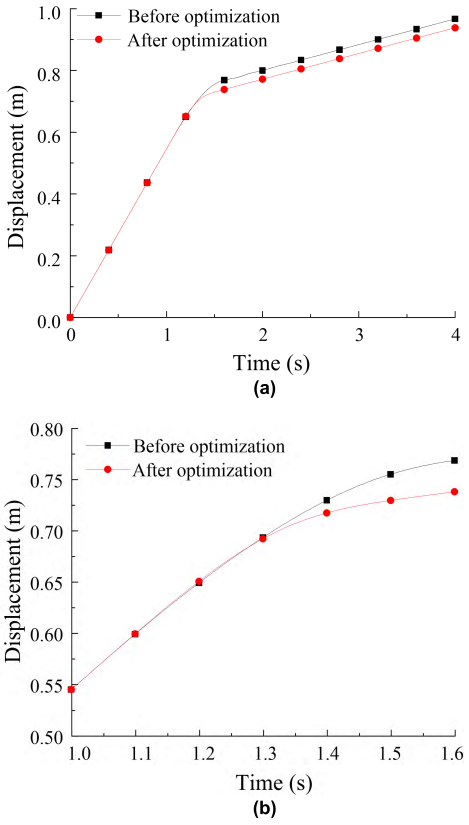

FIGURE 15. Mobile crossbeam displacement curve. (a) Mobile crossbeam displacement during the falling process. (b) Enlarged drawing of (a) in 1 ∼ 1.6s.

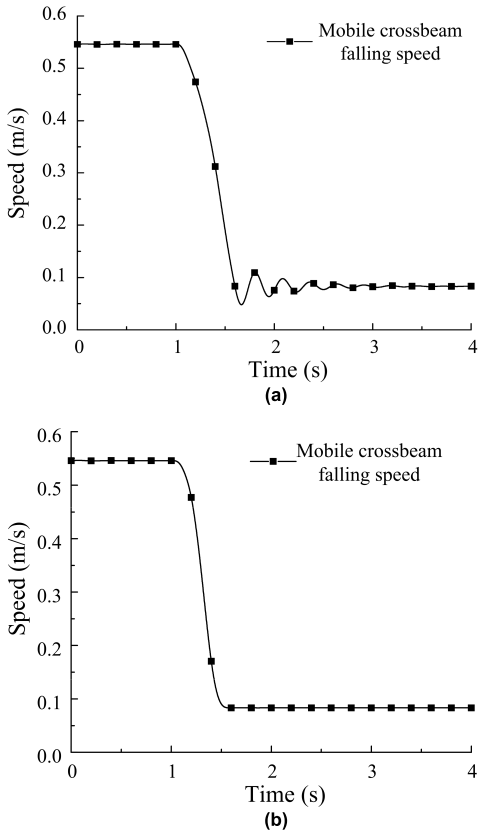

FIGURE 16. Mobile crossbeam velocity curve. (a) Before optimization. (b) After optimization.

The optimized trajectory enables the mobile crossbeam to run fast and smooth to the target speed, which helps the press run more smooth and fast.

It can be seen from Fig. 17 that the uniform speed trajectory will cause the return cylinder pressure fluctuation greatly, and the settling time is too long. In contrast, although the pressure peak of the optimized system pressure curve slightly increases, the settling time is greatly shortened, and the number of pressure oscillation is also obviously reduced.

Based on the system pressure error integral comprehensive index adopted by (25), the optimized system performance is:

$$\frac{J_y(\tilde{p}, u)}{J_0(\tilde{p}, u)} = \frac{483633.7}{975883.5} \times 100\% = 49.56\% \tag{34}$$

It can be seen from (34) that the ITAE index of the optimized spline interpolation trajectory is reduced by 49.56% compared with the uniform speed trajectory within 1 ∼ 4s. This result shows that in the comprehensive index, the fluctuation of system pressure during the settling process is greatly reduced, which effectively suppresses the internal shock and vibration of hydraulic system.

IV. ANALYSIS OF EXPERIMENTAL RESULTS

The mobile crossbeam variable-speed falling experiment will experiment with the research content based on the project cooperation project of the 2500 tons' composite hydraulic press. The main structure of the press uses the three-beam four-column combined frame structure, and the electrical control system adopts the control structure composed of Siemens S7-300 controller and ET-200S slave station. The communication protocol uses PROFIBUS-DP and TCP/IP, and is programmed by STEP 7. The acquisition system uses BAUMER PDRDE002.S14.C460DE pressure sensor and MTS Temposonic GT displacement sensor to monitor the experiment parameters by real-time, and transmits the signal to the upper PC through the NI-USB6218 acquisition card and saves and solves the data by LabVIEW.

A. MODEL IDENTIFICATION EXPERIMENT RESULTS AND ANALYSIS

According to analysis of Fig. 8 ∼ 11, the overall system performance is best when the variable-speed time is around 0.6s. So, we set the variable-speed times of uniform speed trajectory as 0.5s, 0.6s, and 0.7s, and obtain the pressure curve of the return cylinder. The comparison chart between simulation and experiment results are as follows:

Comparing the experimental data with the simulation curve can be obtained Fig. 20 to Fig. 22. These figures show that the simulation results and the experimental results match well in the previous main peak stage. In the process of the return cylinder pressure gradually becoming new steady state,

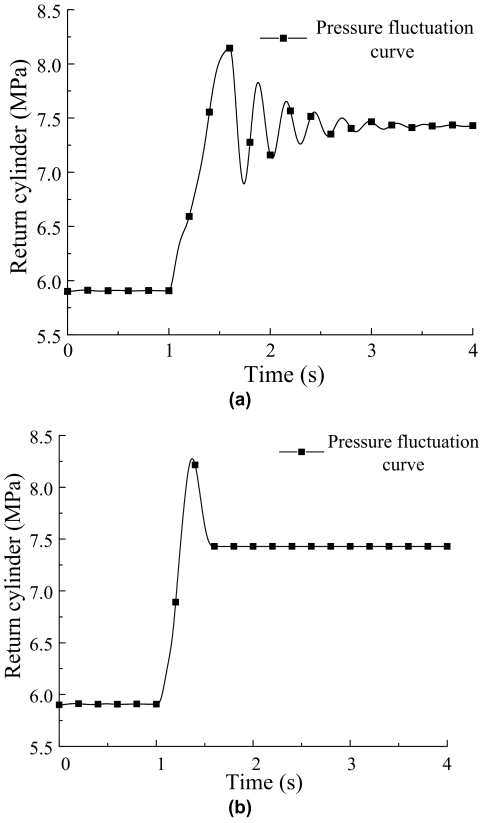

FIGURE 17. Return cylinder pressure fluctuation. (a) Before optimization. (b) After optimization.

FIGURE 18. Mobile crossbeam variable-speed falling system experiment platform.

there is a small deviation of pressure fluctuation. On the one hand, there is a certain deviation in the model training results, on the other hand, the on-site interference will also cause the difference. The simulations and experimental results show that the variable-speed falling dynamic model can reflect the state of the press in actual working conditions, and can predict the model accurately.

B. OPTIMIZATION EXPERIMENT AND ANALYSIS

Based on the optimized variable-speed trajectory, we set the variable-speed time at 0.6s and take the uniform speed trajectory, the simple harmonic trajectory and the optimized

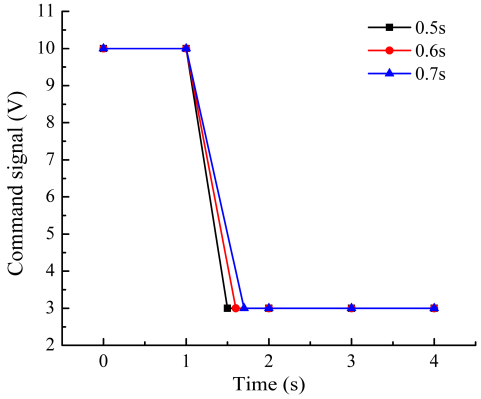

FIGURE 19. Valve command signal.

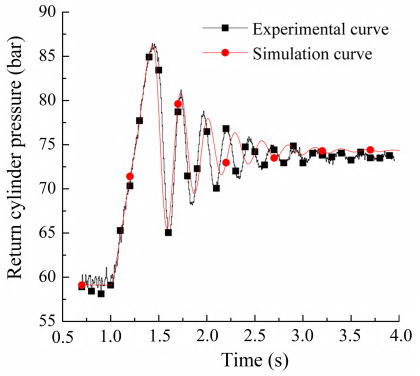

FIGURE 20. Return cylinder pressure comparison (0.5s).

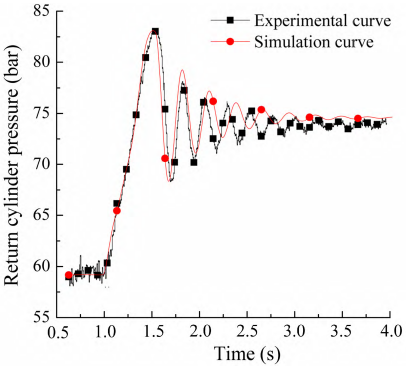

FIGURE 21. Return cylinder pressure comparison (0.6s).

trajectory as the input commands of electro-hydraulic proportional cartridge valve.

Inputting $u_t = 3\text{V}$, $u_0 = 10\text{V}$ and $t_s = 0.6\text{s}$ into (13), we can obtain the uniform speed trajectory:

$$U_{unl}(t) = 10 + \frac{3-10}{0.6}t \tag{35}$$

Inputting $u_t = 3\text{V}$, $u_0 = 10\text{V}$, $t_s = 0.6\text{s}$ and $k = 0$ into (14), we can obtain the simple harmonic trajectory:

$$U_{shm}(t) = \frac{10-3}{2}\cos(\frac{\pi}{0.6}t) + \frac{10+3}{2} \tag{36}$$

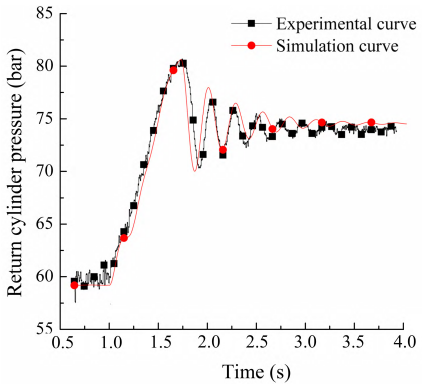

FIGURE 22. Return cylinder pressure comparison (0.7s).

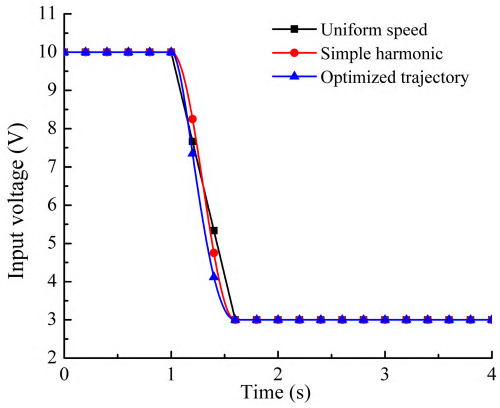

FIGURE 23. Valve command signal.

Using the optimized trajectory in the previous section:

$$U_{spl}(t) = \begin{cases} 183.9412t^3 - 103.1179t^2 + 10, & 0 \le t \le 0.2 \\ 39.7374(t-0.2)^3 + 7.2468(t-0.2)^2 \\ \quad -19.1742(t-0.2) + 7.3468, & 0.2 \le t \le 0.4 \\ -7.7392(t-0.4)^3 + 31.0893(t-0.4)^2 \\ \quad -11.507(t-0.4) + 4.1197, & 0.4 \le t \le 0.6 \end{cases} \tag{37}$$

We perform three trials for each of the three different variable-speed falling trajectories, and collect and record experiment data.

It can be seen from Fig. 23 to Fig. 26 that when the variable-speed time is 0.6s, all three trajectories can track the target command. But there exists 0.4V command deviation during the entire variable-speed process. This is caused by system errors during experiment, and it can be adjusted by the feed-forward compensation during the actual pressing operations. Compared with the uniform speed command trajectory, the other two trajectories have better smoothness during the variable-speed process. The pressure curve taking the uniform speed trajectory as the voltage command has large pressure fluctuation, long settling time and large number

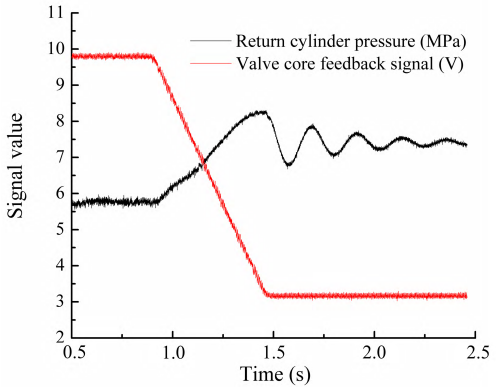

FIGURE 24. Pressure curve of uniform speed trajectory.

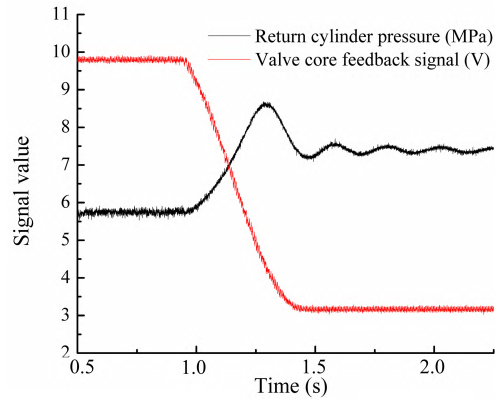

FIGURE 25. Pressure curve of simple harmonic trajectory.

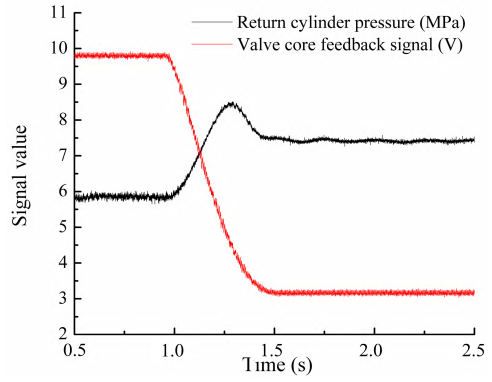

FIGURE 26. Pressure curve of optimized trajectory.

of oscillations. In contrast, the system pressure fluctuations of the simple harmonic trajectory are reduced, but there are still large fluctuations. Using the optimized trajectory as the voltage command, the system pressure fluctuation is significantly reduced compared with the other two, the settling time of return cylinder pressure reaching the new steady-state error band is reduced, so the number of oscillation is.

Table. 4 is obtained from the pressure response curves of three trajectories:

TABLE 4. Experimental data for three trajectories.

Trajectory name	Minimum pressure value (MPa)	Maximum pressure value (MPa)	Maximum pressure fluctuation (MPa)
Uniform speed trajectory	6.80	8.26	1.46
Simple harmonic trajectory	7.20	8.61	1.42
Optimized trajectory	7.37	8.45	1.09
Trajectory name	**Initial fluctuation time (s)**	**Terminal fluctuation time (s)**	**Settling time (s)**
Uniform speed trajectory	0.45	1.96	1.51
Simple harmonic trajectory	0.47	1.80	1.33
Optimized trajectory	0.48	1.04	0.56

As can be seen from Table 4 that the optimized trajectory's vibration settling time is reduced by 62.91% and the maximum pressure fluctuation is reduced by 25.34% compared with the uniform speed trajectory, 57.89% and 23.24% compared with the simple harmonic trajectory.

V. CONCLUSIONS

This paper takes the mobile crossbeam falling process of the composite hydraulic press as the research object, analyzes the key action and characteristic requirements of the mobile crossbeam falling process in detail, and establishes the nonlinear hydraulic system control model. The BP neural network algorithm is used to improve the model accuracy.

Then this paper compares three types of variable-speed falling trajectory (uniform speed trajectory, simple harmonic trajectory and cubic polynomial trajectory), and has the conclusions that the cubic polynomial trajectory is most suitable for mobile crossbeam falling. Next, this paper proposes the command trajectory planning method based on spline interpolation function, and optimizes it globally with improved migration genetic algorithm. The simulation optimization results show that the optimized variable-speed falling trajectory has smaller pressure shock and faster settling speed than the traditional uniform speed trajectory. The system ITAE index is reduced by 49.56%, which can make the mobile crossbeam variable-speed falling process more smooth and shorten the pressing cycle.

Finally, establishing the mobile crossbeam variable-speed falling system experiment platform, the experiment verifies the reliability of nonlinear hydraulic control system model. Comparing the experimental data of three trajectories, the experiment verifies that the vibration suppression ability of the designed trajectory is better than the other two trajectories. The experiment results show that the optimized falling trajectory reduces the settling time by 62.91% and the maximum pressure fluctuation by 25.34% compared with the traditional uniform speed trajectory.

REFERENCES

[1] C. Gerstenberger, T. Osiecki, L. Kroll, P. Scholz, and H. Seidlitz, "Processing and characterization of cathodic dip coated metal/composite-laminates," *Arch. Civil Mech. Eng.*, vol. 16, no. 3, pp. 467–472, 2016.
[2] A. Katunin, "Stone impact damage identification in composite plates using modal data and quincunx wavelet analysis," *Arch. Civil Mech. Eng.*, vol. 15, no. 1, pp. 251–261, 2015.
[3] B. Li, Y. J. Pang, Y. X. Cheng, and X. M. Zhu, "Collaborative optimization for ring-stiffened composite pressure hull of underwater vehicle based on lamination parameters," *Int. J. Naval Archit. Ocean Eng.*, vol. 9, no. 4, pp. 373–381, 2017.
[4] D. A. Grynko, A. N. Fedoryak, P. S. Smertenko, O. P. Dimitriev, N. A. Ogurtsov, and A. A. Pud, "Hybrid solar cell on a carbon fiber," *Nanosc. Res. Lett.*, vol. 11, no. 1, Dec. 2016.
[5] C. C. Zhao, S. F. Yang, P. P. Liu, G. J. Dong, M. Y. Cao, and H. B. Hao, "Principle and theoretical analysis of the balancing system for large die forging hydraulic Press," *J. Mech. Eng.*, vol. 48, no. 10, pp. 82–89, 2012.
[6] Y. T. An, Y. Wang, and F. Cao, "ETMD system in vibration control of control valve and friction compensation," in *Proc. Int. Conf. Elect. Control Eng.*, Jun. 2010, pp. 922–925.
[7] J. Pinho, P. Rambaud, and S. Chabane, "Mass flux and hydrodynamic forces of two-phase cavitating flow through a safety relief valve at initial subcooling conditions," in *Proc. ASME Pressure Vessels Piping Conf.*, Jul. 2014, pp. 20–24.
[8] Y. C. Yang *et al.*, "High fidelity simulation of safety relief valve internal flows," in *Proc. ASME Pressure Vessels Piping Conf.*, Jul. 2015, pp. 19–23.
[9] S. J. Guo, L. Xu, Y. L. Liu, X. X. Guo, and L. Zuo, "Modeling and experiments of a hydraulic electromagnetic energy-harvesting shock absorber," *IEEE/ASME Trans. Mechatronics*, vol. 22, no. 6, pp. 2684–2694, Dec. 2017.
[10] S. J. Cho, J. C. Lee, Y. H. Jeon, and J. W. Jeon, "The development of a position conversion controller for hydraulic Press systems," in *Proc. IEEE Int. Conf. Robot. Biomimetics (ROBIO)*, Dec. 2009, pp. 2019–2022.
[11] F. Guo, J. H. Wei, Q. Zhang, and Y. Xiong, "Hybrid position/pressure control of hydraulic Press based on cascade controller," *J. Zhejiang Univ. Eng. Sci.*, vol. 51, no. 10, pp. 1937–1947, 2017.
[12] B. J. Chen, S. H. Huang, J. F. Gao, and L. Jin, "Control strategy for free forging hydraulic Press," *Chin. J. Mech. Eng.*, vol. 44, no. 10, pp. 304–307+312, 2008.
[13] J. Q. Lou, Y. D. Wei, G. P. Li, Y. L. Yang, and F. R. Xie, "Optimal trajectory planning and linear velocity feedback control of a flexible piezoelectric manipulator for vibration suppression," *Shock Vib.*, vol. 11, Jun. 2015, Art. no. 952708.
[14] M. P. Shreelakshmi and V. Agarwal, "Trajectory optimization for loss minimization in induction motor fed elevator systems," *IEEE Trans. Power Electron.*, vol. 33, no. 6, pp. 5160–5170, Jun. 2018.
[15] M. Ruzzene, R. Kamada, C. L. Bottasso, and F. Scorcelletti, "Trajectory optimization strategies for supercavitating underwater vehicles," *J. Vib. Control*, vol. 14, no. 5, pp. 611–644, 2008.
[16] Y. T. Li, Y. Wu, and X. J. Qu, "Chicken swarm-based method for ascent trajectory optimization of hypersonic vehicles," *J. Aerosp. Eng.*, vol. 30, no. 5, 2017, Art. no. 04017043.
[17] L. Moriello, L. Biagiotti, and C. Melchiorri, "Multidimensional trajectories generation with vibration suppression capabilities: The role of exponential B-splines," *IFAC-PapersOnLine*, vol. 50, no. 1, pp. 6054–6059, 2017.
[18] W. Aribowo and K. Terashima, " Cubic spline trajectory planning and vibration suppression of semiconductor wafer transfer robot arm," *Int. J. Autom. Tech.*, vol. 8, no. 2, pp. 265–274, 2014.
[19] K. Subbarao and B. M. Shippey, "Hybrid genetic algorithm collocation method for trajectory optimization," *J. Guid. Control Dyn.*, vol. 32, no. 4, pp. 1396–1403, 2009.
[20] A. Li, W. Zhao, S. Li, X. Qiu, and X. Wang, "Research on the motion trajectory optimization method based on the improved genetic algorithm for an intelligent vehicle," *Proc. Inst. Mech. Eng. D, J. Automobile Eng.*, vol. 230, no. 13, pp. 1729–1740, 2016.

[21] X. Ren, X. Q. Liu, and Z. Meng, "Trajectory planning algorithm for 3dof electro-hydraulic servo manipulators," in *Proc. 2nd Int. Conf. Comput. Sci. Appl. Eng.*, Oct. 2018, pp. 22–24.
[22] K. He, Y. X. Luo, C. T. Kong, and R. Du, " Trajectory planning, optimization and control of a hybrid mechanical press," *WSEAS Trans. Syst.*, vol. 8, no. 5, pp. 614–627, 2009.
[23] H. Du, Y. Zhang, W. J. Cai, H. Chen, and X. W. Lin, "The trajectory optimization of mobile crossbeam in composite hydraulic Press based on modified multi-island genetic algorithm," *J. Chin. Inst. Eng.*, vol. 40, no. 3, pp. 219–227, 2017.
[24] J. Wang, Y. Wen, Y. Gou, Z. Ye, and H. Chen, "Fractional-order gradient descent learning of BP neural networks with caputo derivative," *Neural Netw.*, vol. 89, pp. 19–30, May 2017.
[25] X. T. Zhou, W. M. Chen, L. Y. Chu, M. G. Yi, and M. H. Chen, "Theoretical study on dynamic filtration with the membrane in simple harmonic motion," *Chin. J. Chem. Eng.*, vol. 12, no. 5, pp. 723–727, 2004.
[26] T. T. Su, L. Cheng, Y. K. Wang, X. Liang, J. Zheng, and H. Zhang, "Time-optimal trajectory planning for delta robot based on quintic pythagorean-hodograph curves," *IEEE Access*, vol. 6, pp. 28530–28539, 2018.
[27] L. Lu, L. Zhang, Y. Gu, and J. Zhao, "Fast parametric curve interpolation with minimal feedrate fluctuation by cubic B-spline," *Proc. Inst. Mech. Eng. B, J. Eng. Manuf.*, vol. 232, no. 9, pp. 1642–1652, 2016.
[28] K. J. Åström, *Introduction to Stochastic Control Theory*. Cleveland, OH, USA: World, 1970.
[29] T. Zhanlav and R. Mijiddorj, "Convexity and monotonicity properties of the local integro cubic spline," *Appl. Math. Comput.*, vol. 293, pp. 131–137, Jan. 2017.
[30] A.K. Gupta, *Numerical Methods Using MATLAB*. Upper Saddle River, NJ, USA: Prentice-Hall, 2000.
[31] J. T. Jia, T. Sogabe, and S. M. Li, "A generalized symbolic Thomas algorithm for the solution of opposite-bordered tridiagonal linear systems," *J. Comput. Appl. Math.*, vol. 290, no. 15, pp. 423–432, 2015.
[32] S. N. Sivanandam and S. N. Deepa, *Introduction to Genetic Algorithm*. Berlin, Germany: Springer, 2008.
[33] A. R. Munoz and I. G. Rodriguez, *Handbook of Genetic Algorithms: New Research*. Hauppauge, NY, USA: Nova Science Publishers, 2012.
[34] D. Gladwin, P. Stewart, and J. Stewart, "A controlled migration genetic algorithm operator for hardware-in-the-loop experimentation," *Eng. Appl. Artif. Intell.*, vol. 24, no. 4, pp. 586–594, 2011.
[35] W.-Z. Dai and K. Xia, "Hybrid genetic algorithm based on chaotic migration strategy for solving flow shop scheduling problem with fuzzy delivery time," *J. Adv. Comput. Intell.Intell. Inform.*, vol. 19, no. 3, pp. 359–364, 2015.
[36] Y. M. Lu, M. Li, L. Li, and H. Y. Yang, "Improved cellular genetic algorithm based on migration of different individuals," *Syst. Eng. Electron.*, vol. 33, no. 3, pp. 690–693, 2011.

HENG DU received the B.S. degree from Tongji University, China, in 2006, and the Ph.D. degree from Zhejiang University, China, in 2011. He joined the School of Mechanical Engineering and Automation, Fuzhou University, China, in 2012, where he is currently an Associate Professor. His current research interests include the theory and application of electro-hydraulic control, multi-axle steering control, and hydraulic press.

ZHIQIANG LIN received the B.Tech. degree from the Qingdao University of Technology, Qingdao, China, in 2017. He is currently pursuing the master's degree with the School of Mechanical Engineering and Automation, Fuzhou University, Fuzhou, China. His current research interest includes the nonlinear servo control of mechatronic systems.

YUAN ZHANG received the M.S. degree in mechanical manufacturing and automation from Fuzhou University, Fuzhou, China, in 2017. He is currently pursuing the Ph.D. degree with the School of Mechanical and Automotive Engineering, South China University of Technology, Guangzhou, China. His research interests are in the fields of robotics and machine vision, image processing, and visual servoing.

HUI CHEN received the B.S. degree from Fujian Agriculture and Forestry University, in 2004, the master's degree from Fuzhou University, in 2007, and the Ph.D. degree form Zhejiang University, in 2011. He joined the School of Mechanical Engineering and Automation, Fuzhou University, China, in 2011, where he is currently an Associate Professor. His current research interests include the heat and mass transfer of fluid systems and the application of electro-hydraulic systems.

ZHIMIN XU received the B.Tech. degree from Fuzhou University, Fuzhou, China, in 2013. He joined Fujian Haiyuan Composites Technology Co., Ltd., Fuzhou, in 2011. His current research interests include the composite presses and electrical automation of composite materials.